All-dielectric photonic higher-order topological insulator induced by a staggered bianisotropy

Xiaoting Sang,[1,*] Junpeng Hou,[2,†] Yazhou Gu,[1] Ya-Jie Wu,[3,4,‡] and Zhitong Li[1,§]

[1]*State Key Laboratory of Information Photonics and Optical Communications, School of Science, Beijing University of Posts and Telecommunications, Beijing 100876, China*

[2]*Pinterest, Inc., San Francisco, California 94107, USA*

[3]*School of Sciences, Xi'an Technological University, Xi'an 710032, China*

[4]*Quantroyi, Inc., Shanghai 200023, China*

(Received 5 December 2023; revised 27 March 2024; accepted 20 May 2024; published 20 June 2024)

In this paper, we introduce a two-dimensional all-dielectric photonic higher-order topological insulator that is driven by the bianisotropic responses of electromagnetic fields. The nontrivial topology originates from staggered bianisotropy effects, which result in modulated coupling between neighbor sites under a fixed lattice constant. This model is generalized from an analogous Su-Schrieffer-Heeger model in one dimension and we show that it realizes a second-order photonic topological insulator with robust symmetry-protected corner modes in two dimensions. We also demonstrate that the topological property of such a model can be characterized by a quantized quadrupolar moment. Our paper introduces a different platform for studying higher-order topological photonics via bianisotropy, as well as a distinct method to engineer all-dielectric topological photonic meta-atoms.

DOI: 10.1103/PhysRevA.109.063518

I. INTRODUCTION

In condensed-matter physics, topological insulators have drawn tremendous research efforts due to their remarkable property of insulating in the bulk while conducting at the boundary, which is dictated by the so-called bulk-edge correspondence [1–3]. The insulating bulk and conducting edge are robust against disorders and defects. Subsequently, the bizarre zoo of topological insulators has been rapidly extended to other quantum and classical systems including cold atoms [4–10], acoustics [11], and photonics [12–20]. In photonic topological insulators, electromagnetic waves can robustly propagate along the boundary of the system against defects and disorders. Photonic analogs of topological phases of matter have been experimentally investigated in a series of topological models such as the one-dimensional (1D) Su-Schrieffer-Heeger (SSH) model [21–23], two-dimensional (2D) quantum Hall model [13,24], as well as Haldane model [25], which are characterized by Zak phase or Chern number.

More recently, higher-order topological models exhibiting lower-dimensional edge modes on hinges or corners have attracted extensive interest [26–41], which further lead to thriving of its photonic counterparts [39,42–51]. Compared to electronic systems, one merit of photonic materials lies in the easy access to non-Hermitian effects, leading to many exotic effects [52–54]. While this can be simply achieved by incorporating active material as gain [55,56] and plasmonic material as loss [57–59], the inevitable intrinsic loss in plasmonic material at optical frequency will definitely spoil the performance of topological photonic devices. Thus, in order to avoid metallic loss, lossless all-dielectric material serves as one of the most desirable platforms to explore topological phenomena in photonics [60].

On the other hand, a straightforward approach to engineer tight-binding models in photonic systems is to design arrays of coupled dielectric cavities [21] or meta-atoms [61]. The photonic modes between two adjacent cavities or meta-atoms can be evanescently coupled and the coupling strength can be harnessed by the distances of the adjacent cavities. Moreover, incorporating other properties can raise more degrees of freedom in controlling the coupling. One example is the bianisotropy effect, which is known as the coupling of electrical and magnetic dipole moments in a photonic cavity [62–64]. When the spatial inversion symmetry of the cavity is broken, the overlapping between electrical and magnetic dipole splits, raising the bianisotropy effects. The strength and sign of the bianisotropy can be tuned by manipulating the cavities with different spatial inversion symmetries. Interestingly, the coupling strength between two cavities with the same bianisotropy is stronger than that with opposite bianisotropies even if the distance is the same (the sign of bianisotropy can be inverted by simply flipping the cavities or meta-atoms). Using the bianisotropic effects, previous studies have demonstrated an analog of the SSH lattice [65,66] and photonic spin Hall effects [64].

This brings up an interesting question: can we realize more broad topological modes like higher-order corner modes using only bianisotropic effects? In this paper, we answer the question affirmatively by proposing a 2D array of coupled dielectric materials with staggered bianisotropy as an

[*]Contact author: jhou@pinterest.com
[†]Contact author: wuyajie@xatu.edu.cn
[‡]Contact author: zhitong.li@bupt.edu.cn
[§]These authors contributed equally to this work.

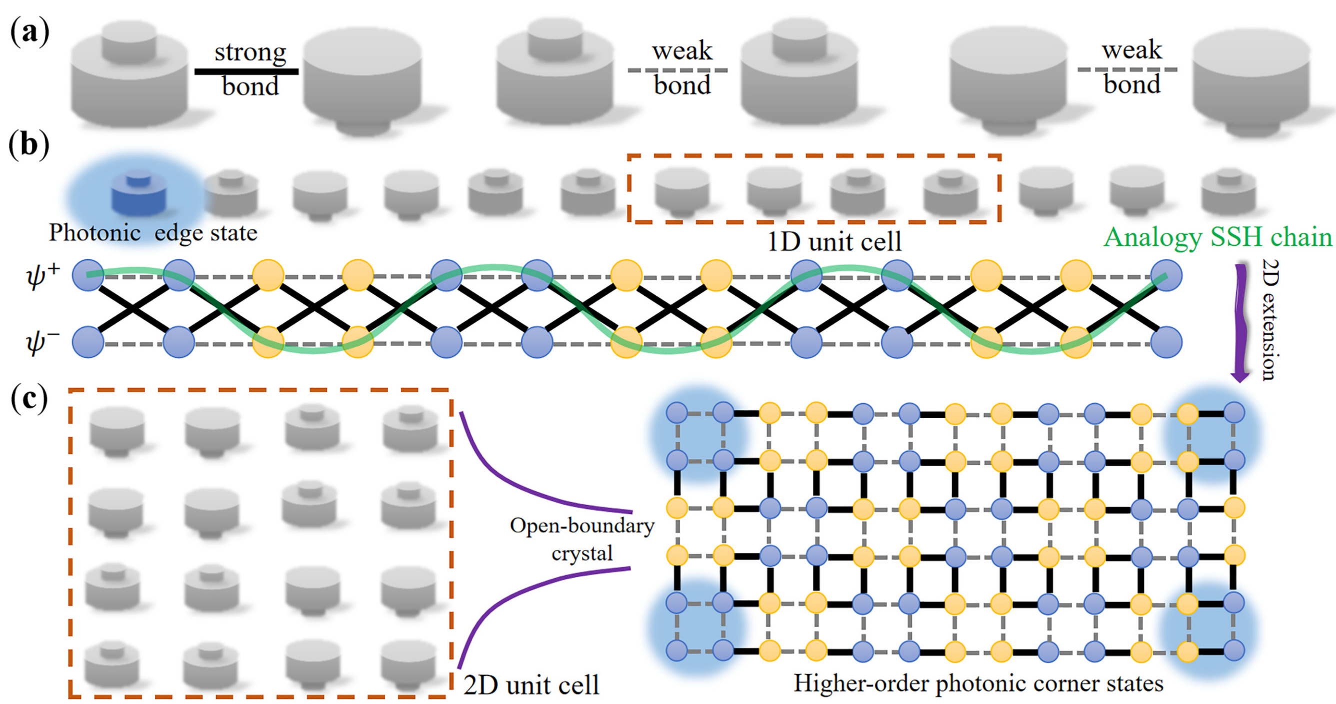

FIG. 1. All-dielectric photonic higher-order topological insulator with staggered bianisotropy. (a) Anisotropy enhances or reduces effective coupling strength when neighboring bianisotropy parameters are different or the same. (b) By taking advantage of the mediated hopping strength, a 1D topological chain with edge states can be realized with staggered bianisotropy, in which an analogy of the SSH model can be extracted along the green curve. (c) The 1D unit cell can be generalized to 2D, realizing a photonic higher-order topological insulator with corner states. The setups shown in the plots provide realistic ways to engineer the higher-order topological insulator proposed in this paper.

all-dielectric photonic second-order topological insulator. The proposed model has some remarkable properties compared to previous proposals for photonic higher-order topological insulators. First of all, it requires no spatial modulations of the distances of adjacent sites, and secondly, it uses only dielectric materials and thus is free from any metallic losses.

The paper is organized as follows. We first review the 1D setup, which is an analogous SSH model, and establish its topological characterization using the non-Abelian Berry phase. We then generalize the 1D chain to a 2D array and reveal the corner modes. We further analyze the symmetry of the Hamiltonian and show that the corners are robust as a result of protection from inversion symmetry. To confirm the topological properties of the corner modes, we also apply the quadrupole moment and find that it is quantized to 0 and 0.5 in the trivial and topological phases.

II. REVISITING THE 1D PHOTONIC LADDER

In this section, we first briefly review the tight-binding model from discrete dipole approximation as discussed in previous work [65]. While it has been pointed out that the staggered bianisotropy parameters lead to effective coupling shown in Fig. 1(a) and, thus, an analogous SSH model, the underlying topological properties and characterizations are not fully investigated. We revisit this problem here more carefully since it is crucial to understanding the 2D generalization.

A. Review of the discrete dipole approximation and tight-binding model

Given the 1D setup shown in Fig. 1(a), we have the dipole moments at site i under the discrete dipole approximation:

$$\boldsymbol{d}_i = \alpha^{ee}\boldsymbol{E}_i + \alpha_i^{em}\boldsymbol{H}_i, \tag{1}$$

$$\boldsymbol{m}_i = \alpha_i^{me}\boldsymbol{E}_i + \alpha^{mm}\boldsymbol{H}_i, \tag{2}$$

where $\boldsymbol{E}_i$ and $\boldsymbol{H}_i$ are electrical and magnetic fields inside the cavity at site i and α notations are polarizability tensors, which are constrained by intrinsic symmetry like time-reversal symmetry and spatial symmetry from the geometry of the cylinders or homogeneous materials. The bianisotropy responses are described by α_i^{em} and α_i^{me}, which may vary from site to site. The electric and magnetic polarizability tensor, α^{ee} and α^{mm}, are diagonal and we assume that out-of-plane dipoles are off-resonant.

Considering only nearest-neighbor hopping, the electromagnetic field can be expanded through dyadic Green functions:

$$\boldsymbol{E}_i = \sum_{i'}\{G^{ee}(\boldsymbol{r}_i - \boldsymbol{r}_{i'})\boldsymbol{d}_{i'} + G^{em}(\boldsymbol{r}_i - \boldsymbol{r}_{i'})\boldsymbol{m}_{i'}\}, \tag{3}$$

$$\boldsymbol{H}_i = \sum_{i'}\{G^{me}(\boldsymbol{r}_i - \boldsymbol{r}_{i'})\boldsymbol{d}_{i'} + G^{mm}(\boldsymbol{r}_i - \boldsymbol{r}_{i'})\boldsymbol{m}_{i'}\}, \tag{4}$$

where $\boldsymbol{r}_i = (x_i, y_i)$ denotes the spatial position of each dipole and $i' = i \pm 1$ represents the nearest neighbor for i in an infinite chain. Keeping only near-field terms, the dyadic Green functions are $G^{em} = G^{me} = 0$, $G_x^{ee} = G_x^{mm} = 2/a^3$, and $G_y^{ee} =$

$G_y^{mm} = -1/a^3$, where a is the lattice constant of the square lattice.

Once we choose a suitable basis for a single disk,

$$|\Psi\rangle = (p_x + im_y, p_x - im_y, m_x + ip_y, m_x - ip_y)^T, \quad (5)$$

where p and m represent the eigenmodes of an isolated disk and the subscripts are for spatial directions. We also arrive at an eigenvalue-form equation:

$$\mu_i \sigma_z^p \psi_i = \left(t_1 \sigma_0^p + t_2 \sigma_x^p\right) \sum_{i'} \psi_{i'}, \quad (6)$$

where $\boldsymbol{\sigma}^p$ is the Pauli matrix acting on the "sublattice" degree of freedom, σ_0^p is the identity matrix, and $\psi_i = (\psi_i^+, \psi_i^-)^T$. We can take the sublattice modes either $\psi^\pm = p_x \pm im_y$ or $\psi^\pm = p_y \pm im_x$ due to the dual symmetry between the meta-atom modes (p_x, m_y) and (p_y, m_x). The parameter μ_i can be tuned by adjusting the lattice spacing a or anisotropy strengths.

It can be shown that the coupling strengths are $t_1 = 1$ and $t_2 = 3$, as visually demonstrated in Fig. 1(a). We want to point out that while the effective coupling can hardly be tuned in experiments, we will assume a general form in this paper to study its topological properties. The important property $t_1 \neq t_2$ ensures that in a realistic setup, the model lies in the topologically nontrivial regions.

B. Topological characterization of the 1D photonic lattice

It was shown that the 1D photonic lattice shown in Fig. 1(b) exhibiting edge modes and the topological origin relates to the SSH model as highlighted by the green curve. Such a structure is referred to as "staggered bianisotropy" in this paper since the signs of the bianisotropic effects are governed by the spatial inversion symmetry and in a single unit cell the signs of the bianisotropic effects are flipped from the second to the third site. While the setup and edge modes in such a 1D chain have been investigated in [65], the topological characterization is less explored. Thus, we reexamine the topological properties of the model more carefully here.

Given the unit cell shown in Fig. 1(b) and assuming the chain is arranged along the x direction, the system Hamiltonian in the momentum space can be written as

$$\begin{aligned} H_{\mathrm{1D}}(k_x) = {} & \mu \sigma_z^x \sigma_0^x \sigma_z^p \\ & + \left[\left(\sigma_0^x \sigma_+^x + \sigma_+^x \sigma_-^x\right)\left(t_1 \sigma_0^p + t_2 \sigma_x^p\right) + \mathrm{H.c.}\right] \\ & + \left[\sigma_+^x \sigma_+^x \left(t_1 e^{-ik_x} \sigma_0^p + t_2 e^{-ik_x} \sigma_x^p\right) + \mathrm{H.c.}\right], \end{aligned} \quad (7)$$

where $\boldsymbol{\sigma}^x$ is the Pauli matrix acting on the degree of freedom spanned along x (chain direction) and the ladder operators are defined by convention $\sigma_\pm = \frac{1}{2}(\sigma_x \pm i\sigma_y)$.

Such a Hamiltonian shows a chiral symmetry $\mathcal{C} H_{\mathrm{1D}}(k_x) \mathcal{C}^{-1} = -H_{\mathrm{1D}}(k_x)$ with $\mathcal{C} = \sigma_0^x \sigma_z^x \sigma_x^p$ so that its spectrum is symmetric to zero. With a trivial time-reversal symmetry $\mathcal{T} H_{\mathrm{1D}}(k_x) \mathcal{T}^{-1} = H_{\mathrm{1D}}(-k_x)$, where $\mathcal{T} = K$ is complex conjugation, we could also define a particle-hole symmetry $\mathcal{P} = \mathcal{C}\mathcal{T}$. Thus unlike the SSH model, which belongs to the AIII class, this model should fall into the BDI class [68]. This is a result that the system can be effectively viewed as two coupled SSH chains so that the time-reversal symmetry is restored.

For a chiral-symmetric system, we can transform the Hamiltonian into an off-diagonal form characterized by a 4×4 matrix $Q(k_x)$ (see Appendix A for details). Since we are dealing with a 1D chain, the usual topological invariant should be the winding number [3]:

$$\nu = \frac{i}{2\pi} \oint dk_x \mathrm{Tr}[Q(k_x)^{-1} dQ(k_x)] \in \mathbb{Z}, \quad (8)$$

which is computed in the 1D momentum space. Yet, such a winding vanishes in all parameter space [65] (see also Appendix A). This is a result that the topological phase transition only happens within each chiral sector, leaving the summation of the winding number of all the sectors, below or above zero, always vanishing. In this sense, $\nu = 0$ is reasonable in electronic systems as the Fermi level is fixed at zero. The edge modes all have nonzero energies here, so it could not be excited in a fermionic system with chiral symmetries.

However, since we are dealing with a photonic system, which is considered bosonic, we need to extend the topological invariant to any gap in the system. Here alternatively, we take the non-Abelian Berry phase as a proper topological invariant, which is defined as

$$\gamma_i = \left(\frac{i}{\pi} \oint dk_x \mathrm{Tr}_i \mathcal{A}(k_x)\right) \mod 2 \in \mathbb{Z}_2, \quad i \in 2\mathbb{Z}, \quad (9)$$

where Tr_i performs partial trace from band 1 to i and the non-Abelian Berry connection $\mathcal{A}_{nm}(k_x) = \langle \phi_n(k_x) | \partial_{k_x} \phi_m(k_x) \rangle$ is defined through the eigenstates $H(k_x)\phi_n(k_x) = E_n(k_x)\phi_n(k_x)$. We then have $\gamma_2 = \gamma_6 = 1$ in the topological region and they vanish in the trivial region, where $i = 2$ and 6 correspond to the gap where the edge modes appear. The topological phase transition and bulk-edge correspondence of the 1D chain are further discussed in more detail in Appendix A.

III. TOWARDS HIGHER-ORDER PHOTONIC CORNER STATES

As we have fully explored the 1D case and revealed its topological nature as two coupled SSH chains, we are ready to reveal its higher-order topology in two dimensions. Here we consider a special case with the unit cell illustrated in Fig. 1(c), which reduces to the 1D chain when projected to either the x or y direction. Previous studies on higher-order topological insulators suggest that a similar generalization of the SSH model to two dimensions renders a second-order topological insulator [26,27]. Here, we expect the staggered strong or weak bonds argument to still apply in two dimensions, making the proposed all-dielectric photonic lattice a potential candidate for a higher-order topological photonic lattice.

A. Photonic corner modes

We first examine the band structure of the photonic lattice on a ribbon geometry, which is shown in Fig. 2(a). Since the spectrum is symmetric to $E = 0$, we only focus on the region $E > 0$. There are two photonic band gaps, which may potentially support the corner modes on a finite sheet. In this specific example, we choose a periodic-boundary condition

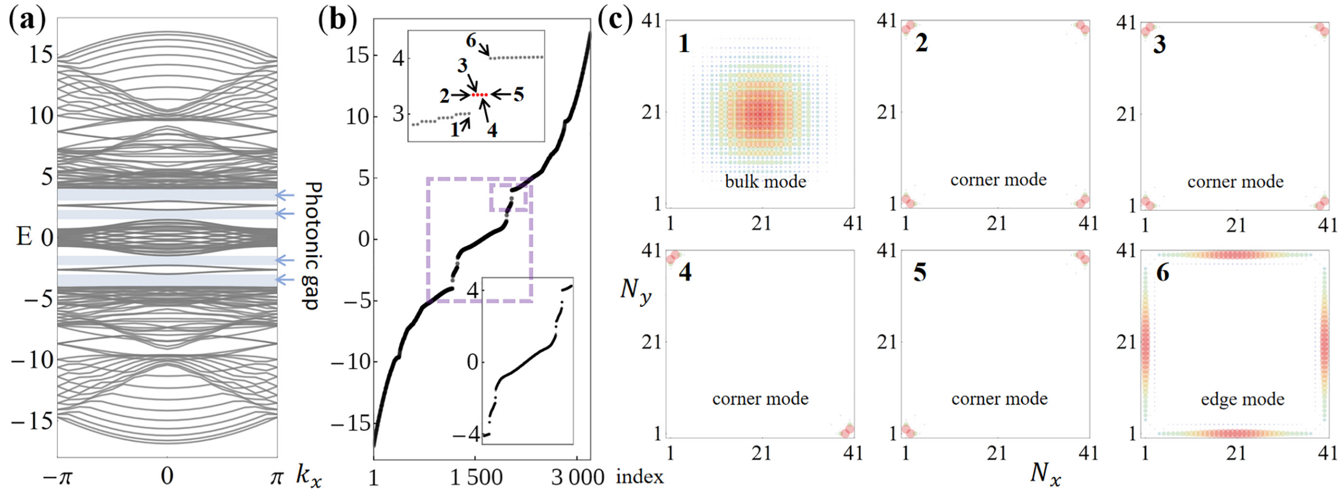

FIG. 2. Higher-order photonic corner states. (a) Band structure on a ribbon sheet with $N_y = 20$ sites along the open-boundary direction. We set $\mu = 4$, $t_1 = 1$, and $t_2 = 3$ for all the panels here. (b) Open-boundary spectrum with $N_x = 40$ and $N_y = 40$. The insets zoom in on the states inside the purple dashed rectangles. All four gaps hold four corner modes and there are no differences among the corner modes within each gap. Thus, we use the corner modes in the top gap for demonstration, which are also highlighted in red in the inset. (c) Spatial distribution of various eigenmodes, which are labeled in the inset of panel (b). The density at a single site is proportional to the radii of the circle.

along x and an open-boundary condition along y while similar results can be observed with k_y.

To further inspect the corner modes, we compute the spectrum on a finite-size sheet with 40×40 sites and it is plotted in Fig. 2(b). We see corner modes are rising in all the gaps and one gap is zoomed in the insets with the four degenerate corner modes being highlighted in red. We label the corner modes, as well as two adjacent bulk modes, from left to right and plot the corresponding electromagnetic field distributions in panel (c). The first bulk mode spreads over the entire crystal with a peak in the middle and decays along the radial directions. The four corner modes occupy only the zero-dimensional corner of the 2D lattice. One interesting property we observed here is that the corner modes are not strictly localized on the corner but on the two closest sites to the corner. This is less common but has been reported in a 2D SSH model with next-nearest-neighbor hopping [67], which shares some common features with our model.

In the next subsection, we will see that these corner modes are protected by spatial symmetries and, thus, are robust to symmetry-preserving disorders. The last one showcases a usual edge mode, which is located at the 1D boundaries of the system. Unlike the in-gap corner modes, such an edge mode can be easily scattered into other bulk modes.

B. System Hamiltonian and symmetry protection

While we have demonstrated the existence of corner modes in the all-dielectric photonic lattice, to gain more insights into the system, we need to first write down its Hamiltonian in momentum space. We adopt similar notations from 1D cases with an extra degree of freedom $\boldsymbol{\sigma}^y$ along y directions, so that the 2D system Hamiltonian reads

$$
\begin{aligned}
H_{2\mathrm{D}}(k_x, k_y) = {}& \mu \sigma_z^y \sigma_0^y \sigma_z^x \sigma_0^x \sigma_z^p \\
&+ \sigma_0^y \sigma_0^y \big[\big(\sigma_0^x \sigma_+^x + \sigma_+^x \sigma_-^x\big)\big(t_1 \sigma_0^p + t_2 \sigma_x^p\big) + \mathrm{H.c.} \big] \\
&+ \sigma_0^y \sigma_0^y \big[\sigma_+^x \sigma_+^x \big(t_1 e^{-ik_x} \sigma_0^p + t_2 e^{-ik_x} \sigma_x^p\big) + \mathrm{H.c.} \big] \\
&+ \big[\big(\sigma_0^y \sigma_+^y + \sigma_+^y \sigma_-^y\big) \sigma_0^x \sigma_0^x \big(t_1 \sigma_0^p + t_2 \sigma_x^p\big) + \mathrm{H.c.} \big] \\
&+ \big[\sigma_+^y \sigma_+^y \sigma_0^x \sigma_0^x \big(t_1 e^{-ik_y} \sigma_0^p + t_2 e^{-ik_y} \sigma_x^p\big) + \mathrm{H.c.} \big],
\end{aligned}
$$

which is a 32×32 matrix.

Such a Hamiltonian possesses a chiral symmetry $\mathcal{C} = \sigma_0^y \sigma_z^y \sigma_0^x \sigma_z^x \sigma_x^p$. Consequently, the symmetric spectra and the definitions of $\mathcal{P}$ and $\mathcal{T}$ symmetries in one dimension are inherited. Besides these three intrinsic symmetries, it is known that higher-order topological states must be protected by spatial symmetries due to the instability of low-dimensional defects on a compact manifold [68,69]. For the 2D bian-isotropic photonic lattice, we have reflection symmetry along x as $\mathcal{R}_x H_{2\mathrm{D}}(k_x, k_y) \mathcal{R}_x^{-1} = H_{2\mathrm{D}}(-k_x, k_y)$, where $\mathcal{R}_x = \sigma_0^y \sigma_0^y \sigma_x^x \sigma_x^x \sigma_x^p$, and similarly, along y with $\mathcal{R}_y = \sigma_x^y \sigma_x^y \sigma_0^x \sigma_0^x \sigma_x^p$. The reflection symmetry operator can be viewed as an operation that exchanges the disks with different anisotropy along one direction, as well as the internal dipole modes. The two reflection symmetries can be further combined to form an inversion symmetry $\mathcal{I} H_{2\mathrm{D}}(k_x, k_y) \mathcal{I}^{-1} = H_{2\mathrm{D}}(-k_x, -k_y)$ and $\mathcal{I} = \mathcal{R}_x \mathcal{R}_y = \sigma_x^y \sigma_x^y \sigma_x^x \sigma_x^x \sigma_0^p$.

While the model itself belongs to the real BDI class by AZ classification [68], we find that $\mathcal{T}\mathcal{I}\mathcal{T}^{-1} = \mathcal{I}$ and $\mathcal{P}\mathcal{I}\mathcal{P}^{-1} = \mathcal{I}$. As a result, this photonic lattice is seemingly trivial by the current classification of higher-order topological insulators [68]. Yet, this is similar to what happens in the 1D ladder model and we will elucidate this by showing that the topological invariant is quantized to nonzero values in the gap where corner modes emerge in the topological phases.

To show the robustness as well as symmetry protection of the corner modes, we apply disorders to the onsite energy split μ and the results are summarized in Fig. 3. In Figs. 3(a) and 3(b), we plot the band structure and the distribution of the corner modes under symmetry-preserving disorders. It is clear that while the exact energy of the corner modes shifts, they remain gapped, degenerate, and localized, regardless of

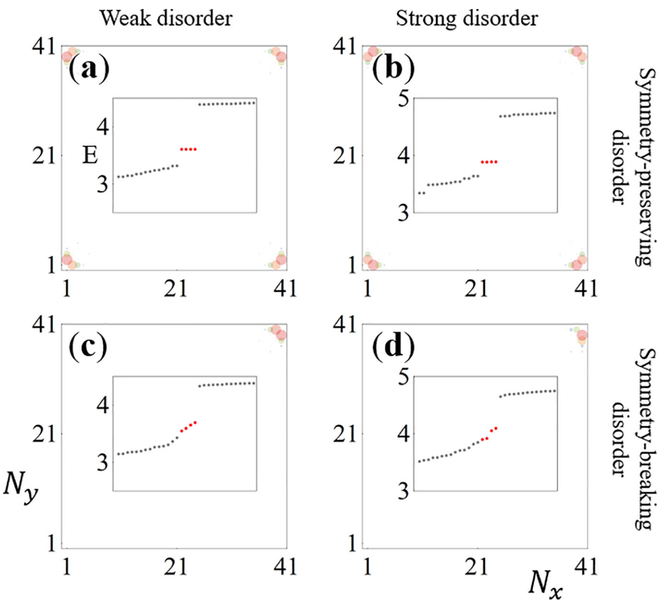

FIG. 3. Corner modes under disorder. The four planes consider all cases combining two axes of the disorders, namely, the strength of the disorder (weak or strong) and symmetry of the disorder (symmetry preserving or breaking). (a) The four corner modes are still degenerate and localized in the corners when a symmetry-preserving disorder is applied in both x and y directions. The panel shows the real-space distribution of the first corner mode (from left to right) while the inset shows the corresponding energy spectrum near the gap, which shifts towards higher energies, compared to the top inset in Fig. 2(b). (b) Similar to panel (a) but with a strong disorder and the corner states still exist. (c), (b) Similar to panels (a) and (c) respectively but plotted using a random disorder that comprises both the inversion symmetry and the reflection symmetries. The degeneracy among the corner modes is broken in both cases and the corner state starts to delocalize in panel (d). The parameters used are the same as Fig. 2.

the strength of the disorder. If the disorder breaks the inversion symmetry discussed above, even a weak disorder can immediately break the degeneracy of the corner modes, as shown in panel (c). As we keep increasing the strength of the disorder, the corner modes start to merge with the bulk modes, indicating they can be easily scattered by defects. This is demonstrated in panel (d) and it is obvious that the state is no longer well localized in the corner.

C. Topological characterization

To this end, we turn to use the quadrupole moment to characterize the topological properties of the proposed model, which can be computed in real space and was shown to be useful in studying amorphous topological insulators [70].

The quadrupole moment is defined as

$$Q_{xy} = (n - n_{\mathrm{AL}}) \mod 1 \in \mathbb{Z}_2, \tag{10}$$

and it is 0 (0.5) for the trivial (topological) phase. The density of the particle can be computed via

$$n = -\frac{i}{2\pi}\mathrm{Tr}\ln U^{\dagger}OU \tag{11}$$

where O is a diagonal matrix with entry $e^{i2\pi x_i y_i/L_x L_y}$ with x_i and y_i the corresponding unit-cell indices and $L_x = N_x/4$ and $L_y = N_y/4$ the number of unit cells along each direction. The matrix U is constructed by arranging columnwise the eigenvectors of N_o occupied states.

To reveal the topological nature underlying n, we need to subtract from it the density at the atomic limit:

$$n_{\mathrm{AL}} = 2n_f \sum_{x_i, y_i} x_i y_i / L_x L_y, \tag{12}$$

where factor 2 comes from the sublattice degree of freedom and $n_f = N_o/2N_xN_y$ is the "filling" of the system.

For the results shown in Fig. 2, there are two different band gaps with four degenerate corner states starting at $E < 0$ and $E > 0$. The sum of the two quadrupole moments at the two gaps is 1 so we only focus on the lower branch. Given the parameters used in Fig. 2, we compute the quadrupole moments up to $N_x = N_y = 120$ and find it to be quantized, $Q_{xy} = 0.5$, confirming the topological nature of the system.

Note that since the corner modes here are protected by inversion symmetries and it was shown that such a system can only belong to a zero or a $\mathbb{Z}_2$ classification [68], the topological invariant Q_{xy} is sufficient to characterize the topological phases.

IV. CONCLUSION AND OUTLOOK

To conclude, we have introduced a class of all-dielectric photonic higher-order topological insulators via engineering staggered bianisotropy, where we do not need to modulate the spatial distance of neighbor lattice sites. We first uncover the topological properties of its 1D counterpart as two coupled SSH lattices and then demonstrate the topological corner modes by directly generalizing the tight-binding model to two dimensions. The system exhibits rich symmetries and multiple photonic band gaps, and each comes with four degenerate photonic corner states. We also show that they are robust under symmetry-preserving disorders. Finally, we compute the quadrupole moment in the real space to confirm its nontrivial bulk topology.

The proposed schema can be easily realized in modern laboratories and it requires only dielectric materials (see Appendix B for a full-wave simulation of the model on a ribbon geometry). The model also has the potential to be further generalized to three dimensions, which may lead to a three-dimensional photonic topological insulator with hinge modes. Our paper provides an example of building an all-dielectric higher-order topological insulator via engineering the bianisotropy within the system and it opens a different avenue to study distinct topological bianisotropic photonic meta-atoms.

ACKNOWLEDGMENTS

J.H. would like to thank C. Zhang for inspiring discussions. Z.L. acknowledges support from Fundamental Research Funds for the Central Universities (Contract No. 2022RC28) and the Opening Foundation of the State Key Laboratory of Information Photonics and Optical Communication (Grant No. IPOC2023ZT03). Y.W. is supported by National Natural Science Foundation of China under Grants No. 12275203 and

No. 12075176, the Scientific Research Program Funded by Natural Science Basic Research Plan in Shaanxi Province of China (Grant No. 2021JM-421), Innovation Capability Support Program of Shaanxi (Grant No. 2022KJXX-42), and 2022 Shaanxi University Youth Innovation Team Project (Grant No. K20220186).

APPENDIX: TOPOLOGICAL INVARIANT OF THE 1D CHAIN

As discussed in the main text, given the chiral symmetry of the system, the Hamiltonian can be written in an off-diagonal form:

$$H_{1D}(k_x) = \begin{pmatrix} 0 & Q(k_x) \\ Q(k_x)^\dagger & 0 \end{pmatrix}, \tag{A1}$$

with the basis in which the chiral symmetry operator $\mathcal{C} = \sigma_0^x\sigma_z^x\sigma_x^p$ is diagonal. The $Q(k_x)$ matrix is found to be

$$Q(k_x) = \begin{pmatrix} \mu & t_+ & 0 & t_+e^{ik_x} \\ t_- & \mu & t_- & 0 \\ 0 & t_+ & -\mu & t_+ \\ t_-e^{-ik_x} & 0 & t_- & -\mu \end{pmatrix}, \tag{A2}$$

where $t_\pm = t_1 \pm t_2$. Now, the winding number can be computed as

$$\begin{aligned} \nu &= \frac{i}{2\pi}\oint dk_x \mathrm{Tr}[Q(k_x)^{-1}dQ(k_x)], \\ &= \frac{i}{2\pi}\int_0^{2\pi} dk_x \frac{2t_-^2t_+^2\sin(k_x)}{\mu^4 + 2t_-^2 - t_-^2\cos(k_x)} \\ &= 0, \end{aligned} \tag{A3}$$

as long as $t_1 \neq t_2$. This superficially contradicts the usual bulk-edge correspondence in a topological insulator, as pointed out by the authors in [65]. However, we would like to emphasize that the usual topological bulk theory still applies here.

To clarify, this can be viewed as a result of different spin statistics. For a fermionic system, the Fermi level must lay at $E = 0$ whenever chiral symmetry is present, and this system would be correspondingly trivial since the edge modes are not zero-energy modes. However, since photons are bosons, we could excite any states far from the "Fermi" level at zero energy and the topological invariant should be counted for the states below that gap. To address this, we compute the non-Abelian Berry phase as formulated in the main text and these results are presented in Fig. 4.

To study the topological phase transition, we assume a tunable t_1 and t_2. For simplicity, we fix $t_1 = 2$ and vary t_2 to induce the phase transition while μ does not affect the topological phase much. Similar to the SSH model, the system is trivial when $t_2 < t_2$ and it experiences a gap closing at $t_2 = t_1$. When $t_2 > t_1$, it enters the topological region. The topological invariant $\gamma_2 = \gamma_6$ is computed in Fig. 4(a) and it is consistent with our description. The band structure for both periodic- and open-boundary conditions in the trivial and topological region is plotted in panels (b) and (c). The gap closing only happens within each chiral sector (the upper of lower two bands) and the top one is depicted in the inset of panel (b). There is a pair of edge states for both $E > 0$ and $E < 0$ and a typical spatial distribution is plotted in the inset of panel (c). Overall, the 1D photonic meta-atoms here can be treated as two coupled SSH chains and, thus, it could support higher-order topological corner modes when generalized in higher dimensions.

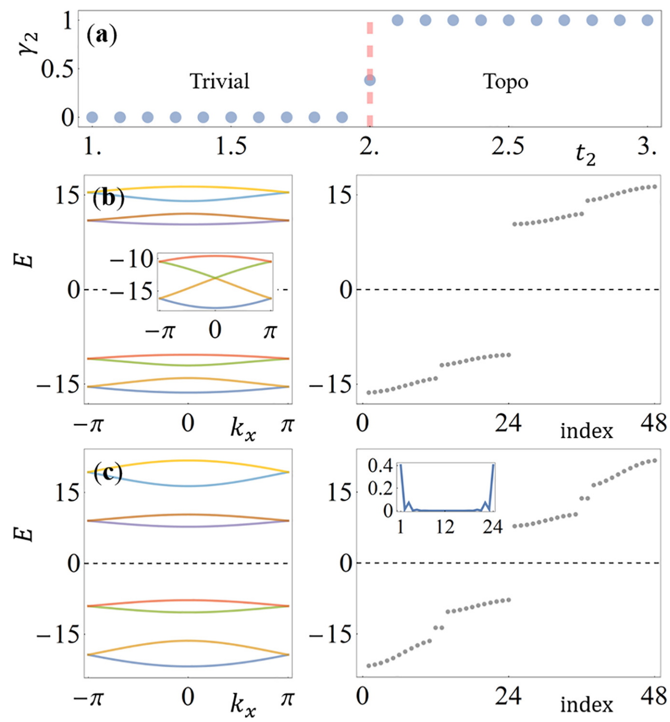

FIG. 4. Topological characterization of the 1D photonic lattice. (a) Topological invariant computed across trivial and topological regions with respect to t_2. The topological phase transition happens at $t_2 = 2$, where an abrupt change of the corresponding topological invariant γ_2 from quantized value 0 to 1 is observed. (b) The band structure (left), as well as the open-boundary spectrum with $N_x = 24$ sites (right), in the trivial region with $t_2 = 1$. The inset shows the upper four bands at the topological phase transition point, where a Dirac point at $k_x = 0$ is observed. (c) Similar to panel (b) but plotted in the topological region $t_2 = 4$, and the inset shows the distribution of the edge modes in real space. The common parameters are chosen as $t_1 = 2$ and $\mu = 13$.

APPENDIX B: FULL-WAVE SIMULATION IN COMSOL

To validate the 2D tight-binding model and to explore the experimental realization of the proposed photonic corner states, we perform a full-wave simulation of the systems in three dimensions using COMSOL MULTIPHYSICS and present the results in this section.

To start with, we need to verify the mode splitting in a single cylinder. In Fig. 5(a), we observe a single characteristic peak corresponding to the overlapping electric and magnetic dipole resonances. When we add a groove as described in the caption, the bianisotropy of the perturbed cylinder leads to two peaks in the scattering spectrum as shown in Fig. 5(b), which is a result of the splitting of the electric and magnetic dipole modes. Now, both modes are coupled and in this specific setup the energy splitting is about 150 MHz while both peaks are still very narrow. Such a choice of parameter corresponds to the topological phase discussed in the main text.

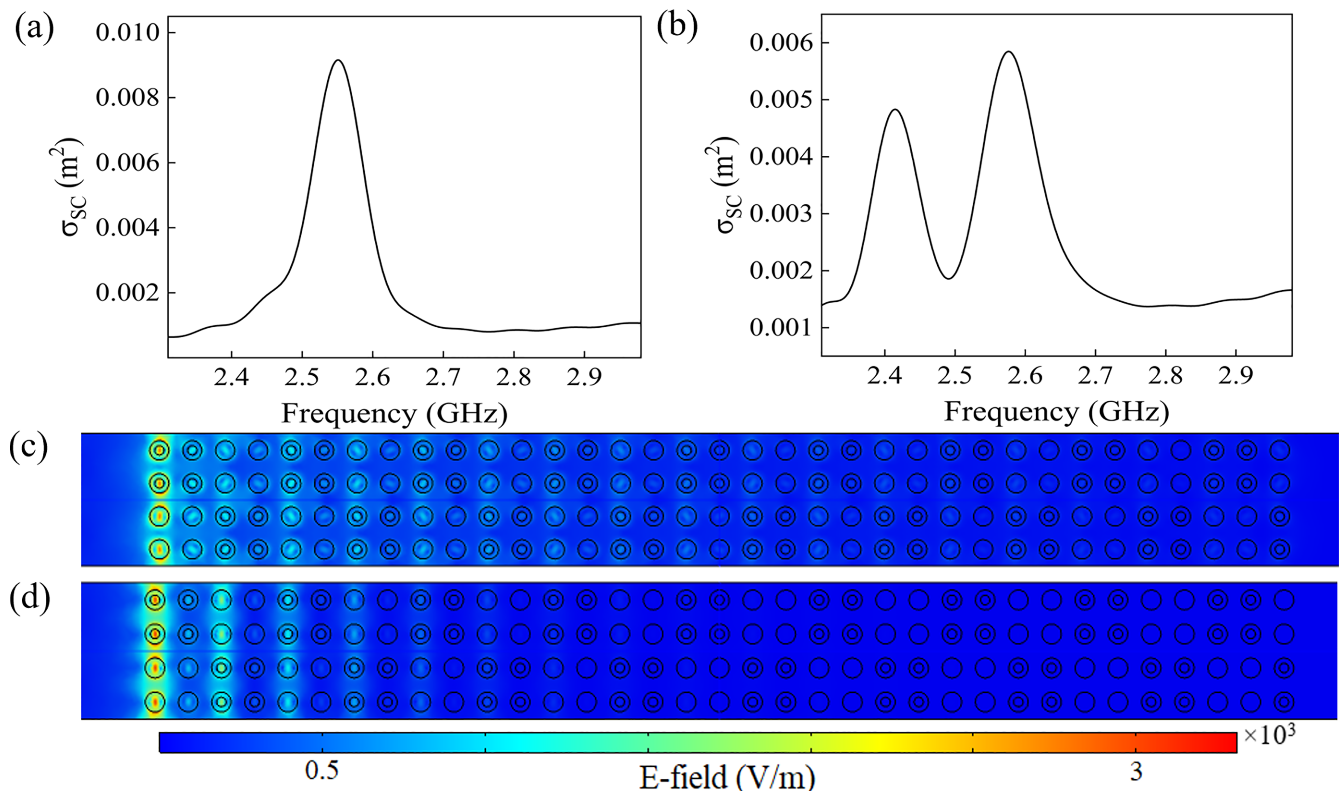

FIG. 5. Three-dimensional full-wave simulation of edge states on a ribbon geometry. (a) The scattering spectrum of a single cylinder with diameter $D_0 = 27.5$ mm and height $H_0 = 11.0$ mm. In all the simulations, we assume high-index dielectric materials with a dielectric constant $\epsilon = 39$. (b) The scattering spectrum of a single cylinder with a cylindrical groove on the top. The diameter and height of the larger cylinder are $D = 29.1$ mm and $H = 11.607$ mm while the groove has a diameter $d = 14$ mm and a depth $h = 1.607$ mm. (c), (d) The real-space distribution or $|E|$ on the $z = 0$ plane of the edge states on a ribbon geometry, i.e., open-boundary condition along x and periodic boundary condition along y. The distance between two adjacent disks is fixed as 5 cm. The corresponding eigenenergies are $2.41 + 0.02i$ and $2.53 + 0.01i$ GHz respectively.

The tight-binding model suggests that we need more than a few unit cells along a given direction with open-boundary conditions to observe the corner modes without observable finite-size effects. In this paper, we set the number of cylinders along such a direction to be 35 so that we have only edge modes on one side. Since the simulation has to be done in three dimensions, it would be too expensive to run a full simulation of a large array of cylinders with open-boundary conditions along both x and y directions. In other words, it is computationally impractical to directly simulate these corner modes. Thus, we need other supporting evidence to verify our theory as well as to guide experiment designs.

To take a step back, we consider cases similar to Fig. 2(a), where we impose open- and periodic-boundary conditions along two spatial directions. This only requires $4 \times 35 = 140$, instead of $35^2 = 1225$, cylinders, making it possible to perform a full simulation in a reasonable time (a few hours to scan a narrow region with given energy ranges). Guided by the results from the tight-binding model, we are able to identify the edge modes depicted in Figs. 5(c) and 5(d). While we cannot directly observe the corner modes with this setup, it helps us narrow down the actual designs of the systems, which means we will be able to measure the corner modes if we can realize such a system using the provided parameters.

The simulation results confirm the results from tight-binding models in the main text and imply that the proposed corner states can be realized in a setup similar to its 1D counterpart with slight modifications of the design of the disks.

[1] D. Xiao, M.-C. Chang, and Q. Niu, Berry phase effects on electronic properties, Rev. Mod. Phys. **82**, 1959 (2010).
[2] X.-L. Qi and S.-C. Zhang, Topological insulators and superconductors, Rev. Mod. Phys. **83**, 1057 (2011).
[3] C.-K. Chiu, J. C. Y. Teo, A. P. Schnyder, and S. Ryu, Classification of topological quantum matter with symmetries, Rev. Mod. Phys. **88**, 035005 (2016).
[4] H. Miyake, G. A. Siviloglou, C. J. Kennedy, W. C. Burton, and W. Ketterle, Realizing the Harper Hamiltonian with laser-assisted tunneling in optical lattices, Phys. Rev. Lett. **111**, 185302 (2013).
[5] M. Atala, M. Aidelsburger, J. T. Barreiro, D. Abanin, T. Kitagawa, E. Demler, and I. Bloch, Direct measurement of the Zak phase in topological Bloch bands, Nat. Phys. **9**, 795 (2013).

[6] M. Aidelsburger, M. Lohse, C. Schweizer, M. Atala, J. T. Barreiro, S. Nascimbéne, N. R. Cooper, I. Bloch, and N. Goldman, Measuring the Chern number of Hofstadter bands with ultracold bosonic atoms, Nat. Phys. **11**, 162 (2015).

[7] G. Jotzu, M. Messer, R. Desbuquois, M. Lebrat, T. Uehlinger, D. Greif, and T. Esslinger, Experimental realization of the topological Haldane model with ultracold fermions, Nature (London) **515**, 237 (2014).

[8] S. Nakajima, T. Tomita, S. Taie, T. Ichinose, H. Ozawa, L. Wang, M. Troyer, and Y. Takahashi, Topological Thouless pumping of ultracold fermions, Nat. Phys. **12**, 296 (2016).

[9] N. Goldman, J. C. Budich, and P. Zoller, Topological quantum matter with ultracold gases in optical lattices, Nat. Phys. **12**, 639 (2016).

[10] N. R. Cooper, J. Dalibard, I. B. Spielman, Topological bands for ultracold atoms, Rev. Mod. Phys. **91**, 015005 (2019).

[11] Z. Yang, F. Gao, X. Shi, X. Lin, Z. Gao, Y. Chong, and B. Zhang, Topological acoustics, Phys. Rev. Lett. **114**, 114301 (2015).

[12] L. Lu, J. D. Joannopoulos, and M. Soljačić, Topological photonics, Nat. Photon. **8**, 821 (2014).

[13] M. A. Bandres, S. Wittek, G. Harari, M. Parto, J. Ren, M. Segev, D. N. Christodoulides, and M. Khajavikhan, Topological insulator laser: Experiments, Science **359**, eaar4005 (2018).

[14] T. Ozawa, H. M. Price, A. Amo, N. Goldman, M. Hafezi, L. Lu, M. Rechtsman, D. Schuster, J. Simon, O. Zilberberg, and I. Carusotto, Topological photonics, Rev. Mod. Phys. **91**, 015006 (2019).

[15] Y. Ota, K. Takata, T. Ozawa, A. Amo, Z. Jia, B. Kante, M. Notomi, Y. Arakawa, and S. Iwamoto, Active topological photonics, Nanophoton. **9**, 547 (2020).

[16] M. Hafezi, E. A. Demler, M. D. Lukin, and J. M. Taylor, Robust optical delay lines with topological protection, Nat. Phys. **7**, 907 (2011).

[17] K. Fang, Z. Yu, and S. Fan, Realizing effective magnetic field for photons by controlling the phase of dynamic modulation, Nat. Photon. **6**, 782 (2012).

[18] Y. E. Kraus, Y. Lahini, Z. Ringel, M. Verbin, and O. Zilberberg, Topological states and adiabatic pumping in quasicrystals, Phys. Rev. Lett. **109**, 106402 (2012).

[19] M. Hafezi, S. Mittal, J. Fan, A. Migdall, and J. M. Taylor, Imaging topological edge states in silicon photonics, Nat. Photon. **7**, 1001 (2013).

[20] K. Takata and M. Notomi, Photonic topological insulating phase induced solely by gain and loss, Phys. Rev. Lett. **121**, 213902 (2018).

[21] M. Parto *et al.*, Edge-mode lasing in 1D topological active arrays, Phys. Rev. Lett. **120**, 113901 (2018).

[22] D. Obana, F. Liu, and K. Wakabayashi, Topological edge states in the Su-Schrieffer-Heeger model, Phys. Rev. B **100**, 075437 (2019).

[23] E. J. Meier, F. A. An, and B. Gadway, Observation of the topological soliton state in the Su-Schrieffer-Heeger model, Nat. Commun. **7**, 13986 (2016).

[24] G. Harari, M. A. Bandres, Y. Lumer, M. C. Rechtsman, Y. D. Chong, M. Khajavikhan, D. N. Christodoulides and M. Segev, Topological insulator laser: Theory, Science **359**, eaar4003 (2018).

[25] Y. G. N. Liu, P. S. Jung, M. Parto, D. N. Christodoulides, and M. Khajavikhan, Gain-induced topological response via tailored long-range interactions, Nat. Phys. **17**, 704 (2021).

[26] W. A. Benalcazar, B. A. Bernevig, and T. L. Hughes, Quantized electric multipole insulators, Science **357**, 61 (2017).

[27] W. A. Benalcazar, B. A. Bernevig, and T. L. Hughes, Electric multipole moments, topological multipole moment pumping, and chiral hinge states in crystalline insulators, Phys. Rev. B **96**, 245115 (2017).

[28] J. Langbehn, Y. Peng, L. Trifunovic, F. von Oppen, and P. W. Brouwer, Reflection-symmetric second-order topological insulators and superconductors, Phys. Rev. Lett. **119**, 246401 (2017).

[29] Z. Song, Z. Fang, and C. Fang, $(d-2)$-Dimensional edge states of rotation symmetry protected topological states, Phys. Rev. Lett. **119**, 246402 (2017).

[30] F. Schindler, A. M. Cook, M. G. Vergniory, Z. Wang, S. S. P. Parkin, B. A. Bernevig, and T. Neupert, Higher-order topological insulators, Sci. Adv. **4**, eaat0346 (2018).

[31] M. Ezawa, Higher-order topological insulators and semimetals on the breathing kagome and pyrochlore lattices, Phys. Rev. Lett. **120**, 026801 (2018).

[32] Q. Wang, C.-C. Liu, Y.-M. Lu, and F. Zhang, High-temperature Majorana corner states, Phys. Rev. Lett. **121**, 186801 (2018).

[33] L. Trifunovic and P. W. Brouwer, Higher-order bulk-boundary correspondence for topological crystalline phases, Phys. Rev. X **9**, 011012 (2019).

[34] C.-H. Hsu, P. Stano, J. Klinovaja, and D. Loss, Majorana Kramers pairs in higher-order topological insulators, Phys. Rev. Lett. **121**, 196801 (2018).

[35] S. A. A. Ghorashi, X. Hu, T. L. Hughes, and E. Rossi, Second-order Dirac superconductors and magnetic field induced Majorana hinge modes, Phys. Rev. B **100**, 020509 (2019).

[36] Y.-J. Wu, J. Hou, Y.-M. Li, X.-W. Luo, and C. Zhang, In-plane Zeeman field induced Majorana corner and hinge modes in an s-wave superconductor heterostructure, Phys. Rev. Lett. **124**, 227001 (2020).

[37] A. B. Wladimir, Li Tianhe and L. H. Taylor, Quantization of fractional corner charge in C_n-symmetric higher-order topological crystalline insulators, Phys. Rev. B **99**, 245151 (2019).

[38] C. W. Peterson, W. A. Benalcazar, T. L. Hughes, and G. Bahl, A quantized microwave quadrupole insulator with topologically protected corner states, Nature (London) **555**, 346 (2018).

[39] A. E. Hassan, F. K. Kunst, A. Moritz, G. Andler, and E. J. Bergholtzl, Corner states of light in photonic waveguides, Nat. Photon. **13**, 697 (2019).

[40] M. Li, D. Zhirihin, M. Gorlach, X. Ni, D. Filonov, A. Slobozhanyuk, A. Alú, and A. B. Khanikaev, Higher-order topological states in photonic kagome crystals with long-range interactions, Nat. Photon. **14**, 89 (2020).

[41] B. Xie, H. Wang, X. Zhang, P. Zhan, J. H. Jiang, M. Lu, and Y. Chen, Higher-order band topology, Nat. Rev. Phys. **3**, 520 (2021).

[42] M. Ezawa, Nonlinear non-Hermitian higher-order topological laser, Phys. Rev. Res. **4**, 013195 (2022).

[43] M. Kim, Z. Jacob, and J. Rho, Recent advances in 2D, 3D and higher-order topological photonics, Light Sci. Appl. **9**, 130 (2020).

[44] X.-W. Luo and C. Zhang, Higher-order topological corner states induced by gain and loss, Phys. Rev. Lett. **123**, 073601 (2019).
[45] B.-Y. Xie, H.-F. Wang, H.-X. Wang, X.-Y. Zhu, J.-H. Jiang, M.-H. Lu, and Y.-F. Chen, Second-order photonic topological insulator with corner states, Phys. Rev. B **98**, 205147 (2018).
[46] M. Serra-Garcia, V. Peri, R. Süsstrunk, O. R. Bilal, T. Larsen, L. G. Villanueva, and S. D. Huber, Observation of a phononic quadrupole topological insulator, Nature (London) **555**, 342 (2018).
[47] T. Liu, Y.-R. Zhang, Q. Ai, Z. Gong, K. Kawabata, M. Ueda, and F. Nori, Second-order topological phases in non-Hermitian systems, Phys. Rev. Lett. **122**, 076801 (2019).
[48] X.-D. Chen, W.-M. Deng, F.-L. Shi, F.-L. Zhao, M. Chen, and J.-W. Dong, Direct observation of corner states in second-order topological photonic lattice slabs, Phys. Rev. Lett. **122**, 233902 (2019).
[49] B.-Y. Xie, G.-X. Su, H.-F. Wang, H. Su, X.-P. Shen, P. Zhan, M.-H. Lu, Z.-L. Wang, and Y.-F. Chen, Visualization of higher-order topological insulating phases in two-dimensional dielectric photonic lattices, Phys. Rev. Lett. **122**, 233903 (2019).
[50] S. Mittal, V. V. Orre, G. Zhu, M. A. Gorlach, A. Poddubny, and M. Hafezi, Photonic quadrupole topological phases, Nat. Photon. **13**, 692 (2019).
[51] L. Zhang, Y. Yang, P. Qin, Q. Chen, F. Gao, E. Li, J.-H. Jiang, B. Zhang, and H. Chen, Higher-order photonic topological states in surface-wave photonic lattices, Adv. Sci. **7**, 1902724 (2020).
[52] R. El-Ganainy, M. Khajavikhan, D. N. Christodoulides, and S. K. Ozdemir, The dawn of non-Hermitian optics, Commun. Phys. **2**, 37 (2019).
[53] H. Zhao, X. Qiao, T. Wu, B. Midya, S. Longhi, and L. Feng, Non-Hermitian topological light steering, Science **365**, 1163 (2019).
[54] J. Hou, Z. Li, X.-W. Luo, Q. Gu, and C. Zhang, Topological bands and triply-degenerate points in non-Hermitian hyperbolic metamaterials, Phys. Rev. Lett. **124**, 073603 (2020).
[55] Z. Li, X.-W. Luo, and Q. Gu, Topological on-chip lasers, APL Photon. **8**, 070901 (2023).
[56] Z. Li, X.-W. Luo, D. Lin, A. Gharajeh, J. Guo, C. Zhang, and Q. Gu, Topological microlaser from non-Hermitian topological bulk, Phys. Rev. Lett. **131**, 023202 (2023).
[57] L. Feng, Z. J. Wang, R.-M. Ma, Y. Wang, and X. Zhang, Single-mode laser by parity-time symmetry breaking, Science **346**, 972 (2014).
[58] M. Pan, H. Zhao, P. Miao, S. Longhi, and L. Feng, Photonic zero mode in a non-Hermitian photonic lattice, Nat. Commun. **9**, 1308 (2018).
[59] Z. Li and Q. Gu, Topological hyperbolic metamaterials, Nanophoton. **13**, 825 (2024).
[60] J. Hou, Z. Li, Q. Gu, and C. Zhang, Topological and hyperbolic dielectric materials from chirality-induced charge-parity symmetry, Phys. Rev. A **104**, 043510 (2021).
[61] S. Jahani and Z. Jacob, All-dielectric metamaterials, Nat. Nanotechnol. **11**, 23 (2016).
[62] A. Slobozhanyuk, S. Hossein Mousavi, X. Ni, D. Smirnova, Y. S. Kivshar, and A. B. Khanikaev, Three-dimensional all-dielectric photonic topological insulator, Nat. Photon. **11**, 130 (2017).
[63] R. Alaee, M. Albooyeh, A. Rahimzadegan, M. S. Mirmoosa, Y. S. Kivshar, and C. Rockstuhl, All-dielectric reciprocal bianisotropic nanoparticles, Phys. Rev. B **92**, 245130 (2015).
[64] D. V. Zhirihin, S. V. Li, D. Y. Sokolov, A. P. Slobozhanyuk, M. A. Gorlach, and A. B. Khanikaev, Photonic spin Hall effect mediated by bianisotropy, Opt. Lett. **44**, 1694 (2019).
[65] D. A. Bobylev, D. A. Smirnova, and M. A. Gorlach, Photonic topological states mediated by staggered bianisotropy, Laser Photon. Rev. **15**, 1900392 (2021).
[66] A. A. Gorlach, D. V. Zhirihin, A. P. Slobozhanyuk, A. B. Khanikaev, and M. A. Gorlach, Photonic Jackiw-Rebbi states in all-dielectric structures controlled by bianisotropy, Phys. Rev. B **99**, 205122 (2019).
[67] X.-W. Xu, Y.-Z. Li, Z.-F. Liu, and A.-X. Chen, General bounded corner states in the two-dimensional Su-Schrieffer-Heeger model with intracellular next-nearest-neighbor hopping, Phys. Rev. A **101**, 063839 (2020).
[68] E. Khalaf, Higher-order topological insulators and superconductors protected by inversion symmetry, Phys. Rev. B **97**, 205136 (2018).
[69] M. Geier, L. Trifunovic, M. Hoskam, and P. W. Brouwer, Second-order topological insulators and superconductors with an order-two crystalline symmetry, Phys. Rev. B **97**, 205135 (2018).
[70] A. Agarwala, V. Juricic, and B. Roy, Higher-order topological insulators in amorphous solids, Phys. Rev. Res. **2**, 012067(R) (2020).